THE JOURNAL OF PHYSICAL CHEMISTRY C

Article

Cite This: J. Phys. Chem. C 2018, 122, 9141−9151

pubs.acs.org/JPCC

Lowest-Energy Crystalline Polymorphs of P3HT

Andriy Zhugayevych,*[,†] Olga Mazaleva,[†] Artem Naumov,[†] and Sergei Tretiak*[,†,‡]

[†]Skolkovo Institute of Science and Technology, Moscow 143026, Russia

[‡]Theoretical Division and Center for Integrated Nanotechnologies, Los Alamos National Laboratory, Los Alamos, New Mexico 87545, United States

Supporting Information

ABSTRACT: We systematically study low-energy crystalline polymorphs of the archetypal conjugated polymer, regioregular poly-3-hexylthiophene (rr-P3HT) using the best available density functional theory methods benchmarked against the ab initio coupled cluster method. A comprehensive conformational search is performed for two-dimensional π-stacks being the most rigid structural unit of bulk P3HT. We have identified a number of nearly isoenergetic polymorphs below the energy level of room-temperature amorphous structures and well below the energy of optimized best-fit experimental models. Classical molecular dynamics simulations show that these crystals retain their structure at least at 200 K. At room temperature, although the conjugated backbone of the π-stack remains ordered, aliphatic side chains are melted, transforming from low-energy folded conformations to high-entropy fully unfolded structures. Our study shows that P3HT is a statistically frustrated system with multiple competing interactions, which complicates fabrication of highly ordered bulk forms but gives structural flexibility of glasses.

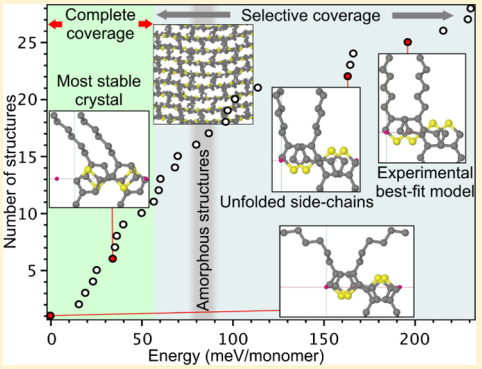

INTRODUCTION

Poly-3-hexylthiophene (P3HT) is a workhorse of modern organic electronics. Despite a modest intrinsic performance, owing mostly to high bandgap and relatively low hole mobility, the highly developed processing protocols of this material make it commonly usable in various prototype devices as well as in basic research seeking structure−property relationships. Numerous studies have provided a detailed understanding of P3HT structure at various scales down to atomic resolution.[1−4] Yet at the smallest scale, the atomistic structure of P3HT evades a complete resolution because of substantial intrinsic disorder and related fundamental challenges in growing perfectly ordered crystals.[5,6] In particular, little is known about low-energy polymorphs of a crystalline regioregular P3HT (rr-P3HT). Here, the regioregularity means ordered attachment of alkyl chains along the polymer, see Figure 1, which is essential for constructing an ideal crystal. Although the mesoscale structure of a material may be unsusceptible to subtle microscopic variations, electronic properties are sensitive to small changes in intrachain and intermolecular packings,[7] requiring accurate knowledge of atomic positions. A recent discovery of two electronically different coexisting aggregates of P3HT[8] is an example of such phenomena.

The mesoscopic structure of P3HT material is determined by several levels of packing, as shown in Figure 1. The smallest building block is the π-stack of individual polymer chains. It is relatively rigid due to covalent bonds along the chain and strong (by contact area) noncovalent bonding between the chains. These two-dimensional layers are packed into a bulk solid by noncovalent interactions between side chains. In most of the observed P3HT morphologies, side chains are not interdigitated, which is referred to as type-1 packing (form I). The resulting three-dimensional structure can grow along the two "noncovalent" directions: π-stacking and side-chain contacts, thus forming tiles (lamellae in polymer physics[9]), whose principal facets are terminated by broken or folded polymer chains referred to as ties. Finally, the lamellar packing of such tiles determine the mesoscopic structure of P3HT.[1] Other nanoscale morphologies exist, including aggregates[8] and epitaxial layers,[1] which may have different mesoscale ordering, whereas the π-stacking seems to be the common structural motif for most of the known forms of P3HT. Another argument to consider π-stack as a fundamental building block of P3HT stems from the electronic structure: strong electronic couplings between monomers inside the π-stack form a continuous two-dimensional network, whereas couplings between π-stacks are negligible[10] except for incoherent Förster energy transfer through space or charge carrier hopping through tie chains.

To resolve P3HT structure at the smallest scale, many structural studies by different techniques have been conducted, including electron diffraction,[11] X-ray diffraction augmented with NMR crystallography,[12] cryotransmission electron microscopy,[3] and other methods.[6,13] These experiments typically directly measure only unit cell parameters, whereas atomic positions are estimated by best-fit modeling.[5,11,12] Indirect

Received: November 14, 2017
Revised: March 27, 2018
Published: March 29, 2018

DOI: 10.1021/acs.jpcc.7b11271
J. Phys. Chem. C 2018, 122, 9141−9151

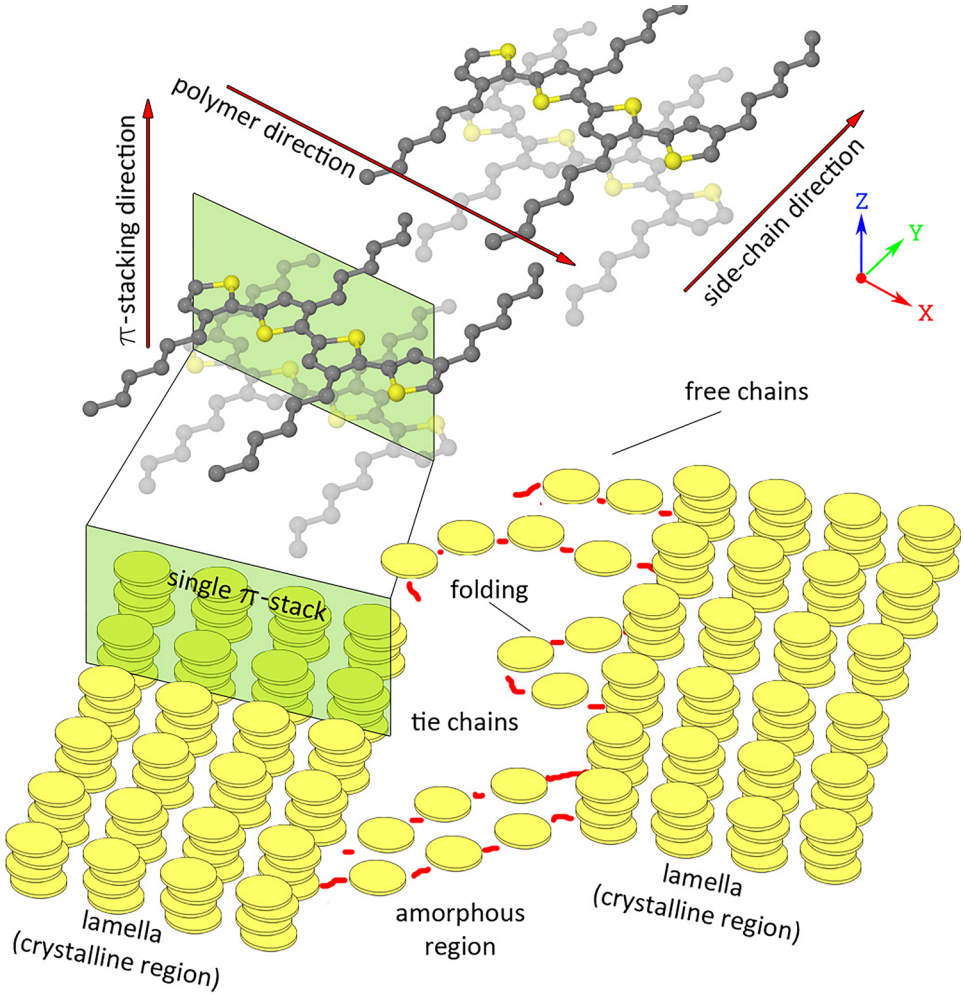

Figure 1. P3HT structure with four levels of packing: polymer, π-stack, interstack packing by side-chains into lamellae, and lamellar packing.

methods, such as inelastic neutron spectroscopy,[5] Raman spectroscopy,[14] and solid-state nuclear magnetic resonance,[6] provide useful restrictions on possible atomic arrangements, but they still require an a priori predicted set of structures. Available experimental data suggest a monoclinic cell with the space group $P2_1/c$.[6,11] Reported cell parameters vary within several percents; see Table 1. The value of the monoclinic angle is somewhat uncertain, but all recently reported values deviate from the right angle by less than 6°, which is the angle obtained by shifting adjacent π-stacks by half of the $\pi-\pi$ distance. This is consistent with absence of specific interactions between π-stacks in type-1 packing (no strong correlations between intra- and inter-π-stack orders). Instead, the stacks pack as textured bricks. Values of other geometric parameters, such as the setting angle and side-chain dihedrals, vary substantially from report to report, e.g., the setting angle is almost 0 in ref 12 and is about 30° in ref 11. In addition, it is unclear if the reported atomic positions correspond to a minimum of potential energy surface (PES) or to an ensemble average of multiple local arrangements.[6,15] This concerns side-chain conformations, setting angle, and interpolymer packing. In particular, it is unclear if regioregular polymer chains are π-stacked regularly (all reported unit cells have antiparallel stacking) or have random forward–backward orientation.

Reported systematic computational studies of semicrystalline P3HT are mostly based on classical molecular dynamics (MD).[22−26] Although yet to be able to sample the entire conformational space of bulk P3HT, existing density functional theory (DFT) calculations generally converge to a few polymorphs of interest.[5,27,28] All such recent investigations focus on the same structural motif consistent with available experimental results. At the same time, no consensus has been achieved on atomic positions within the unit cell, neither is there a common parameterization of the P3HT geometry to differentiate and categorize that zoo of structures available in the literature. It seems natural for polymers that the origin of such diversity is a pronounced polymorphism, so that local atomic arrangements are sensitive to variations in processing conditions or computational methods.[22] Several force field parameterizations have been developed for P3HT using DFT calculations of intramolecular blocks, such as dihedrals and atomic charges, giving reasonable geometry compared to available experimental data.[23,29−33] Yet the main concern of classical force fields is accuracy: although most of the structural features observable experimentally at elevated temperatures are well reproduced in modern simulations, the accuracy of atomic positions is uncertain without reliable validation by experimental or ab initio data, both of which are too scarce today.

Thus, after decades of experimental and theoretical study of P3HT, we are still lacking precise knowledge of its possible microstructures at the scale of individual atom positions in bulk material. Motivated by this need, here we perform a systematic

DOI: 10.1021/acs.jpcc.7b11271
J. Phys. Chem. C 2018, 122, 9141−9151

Table 1. Recently Reported Parameters of P3HT Unit Cell (in Chronological Order) Along with Relevant Results from the Present Work[a]

method	polymer (Å)	π-stack (Å)	side-chain (Å)	angle (deg)
Type-1 Structures				
X-ray + AFM[16]	7.7	7.7	16.8	90
X-ray, str. 1[17]	7.6	7.8	17.2	105*
X-ray, str. 2[17]	7.6	7.7	16.9	100.7*
X-ray[18]	7.7	7.7	15.7	87
ED[11]	7.8	7.8	16.0	86.4
X-ray + NMR[12]	7.7	7.6	16.4	87
cryo-TEM[3]		7.6	17	
X-ray + ED[19]	7.6	7.8	16.7	85
str.[12] at 300 K	7.68	8.2	16.0	95.0
str.[12] by OPLS	7.78	7.1	18.3	94.5
str.[12] by PBE-MBD	7.79	7.1	17.9	88.9
str.[12] by vdW-DF2	7.86	7.4	17.2	86.5
Interdigitated (Type-2) Structure				
ED, str. P3HT-26[20]		9.3	13.1	68.5
X-ray[21]		8.8	12.0	
this work (OPLS)	7.81	8.7	13.2	70.2
this work (PBE-MBD)	7.80	8.9	13.3	69.9
this work (vdW-DF2)	7.89	9.1	13.5	69.3

[a]The three translation vectors are labeled as follows: "polymer" means direction along the polymer; the angle is between "π-stack" and "side-chain" axes except for the two values labeled by asterisk where the angle is between polymer and side-chain axes. The "str.[12]" is the crystal structure reported in ref 12. The unit cell "at 300 K" is simulated by molecular dynamics (MD); the other calculated structures are optimized by the indicated method.

DFT-based scan of a low-energy high-symmetry region of conformational space of bulk rr-P3HT to resolve the uncertainties discussed above and to provide reference data for follow-up studies by improved force fields and multiscale modeling. We start with benchmarking best available DFT methods using high-level theory and experimental crystal data for P3HT and its fragments. Then, we develop a coarse-grained model of P3HT, allowing for efficient parameterization of various crystalline polymorphs as well as for recognition of local structural patterns in amorphous phases. Using the developed methodology, we search for low-energy polymorphs of rr-P3HT, targeting a complete coverage below the energy level of known room-temperature polymorphs and, in addition, within the energy basins of all experiment-derived atomistic models.[11,12,20] After comprehensive sampling of P3HT microstructures, we analyze them to understand common structural motifs of rr-P3HT. Also, we address specific questions related to possible interpretations of best-fit models, use of vibrational spectra to distinguish polymorphs, and understanding of glass forming properties of rr-P3HT, including transition from low-energy to room-temperature structures.

COMPUTATIONAL METHODOLOGY

To get accurate description of bulk P3HT at a relevant spatial scale, we apply a combination of three approaches: ab initio coupled cluster method, DFT, and classical force field. As the reference method, we use explicitly correlated local coupled cluster theory with single, double, and perturbative triple excitations DF-LCCSD(T)-F12,[34] as implemented in MOLPRO program.[35,36] The computations are performed with the cc-pVTZ[37,38] orbital basis set and cc-pVTZ/MP2fit and cc-pVTZ/JKfit basis sets for density fitting. We refer to this method as CCSD(T)/cc-pVTZ.

The main results of this work are obtained at the DFT level. Here, proper choice of the density functional is critical.[39,40] Consequently, a preselected set of functionals is benchmarked against CCSD(T) using representative fragments of P3HT, including its monomer and oligomers of polyethylene and polythiophene, with emphasis on noncovalent interactions and π-conjugated dihedrals. We assess several density functionals commonly applied to π-conjugated molecules: B3LYP, CAM-B3LYP, LC-ωPBE, and ωB97X.[39−41] Noncovalent interactions are of primary importance for P3HT structure; therefore, dispersion corrections are added to these DFT models.[42] We use the D3 correction with Becke−Johnson damping,[43] except for ωB97X, which is considered in ωB97XD version.[44] In the selection of a basis set, we use the minimalist approach to be able to efficiently model bulk P3HT. We test several Pople's basis sets ranging from the minimally acceptable 6-31G*[39,45] up to 6-311+G(3df,2p). All molecular DFT calculations are performed using Gaussian 09 program.[46] To simulate bulk P3HT in a super cell, we need to apply periodic boundary conditions, which are not implemented for the dispersion-corrected functionals in Gaussian 09. For this type of calculation, we use the plane-wave basis with two methods: vdW-DF2[47,48] and many-body dispersion (MBD)-rsSCS,[49] referred here as Perdew−Burke−Ernzerhof (PBE)-MBD. The former method is based on nonlocal correlation functional, accounting for van der Waals interactions with rPW86[50,51] exchange term. It was shown to be accurate in predicting the structure of organic crystals.[52−54] PBE-MBD represents another way for accounting dispersion interactions using PBE[55] density functional coupled with many-body Tkatchenko−Scheffler van der Waals model. It employs range separation of the self-consistent screening of polarizabilities so that the long-range correlation energy can be separated from the short-range functional contribution. Calculations with the plane-wave basis are performed in VASP 5.4 program.[56] More specifically, we use VASP-default PAW pseudopotentials[57] and 600 eV energy cutoff. Γ-Centered Monkhorst−Pack grid with at least 30 k-points per $Å^{-1}$ is fixed for all polymorphs under comparison. Geometry optimization is performed with tight criteria predefined in both Gaussian and VASP programs. In VASP maximum gradients typically do not exceed 20 meV/Å for PBE-MBD and 10 meV/Å for vdW-DF2. Unit cells are optimized using fourth-order polynomial fit of energy for a set of fixed-volume relaxations.

The results of assessment of density functionals are summarized in Table 2 (see the Supporting Information for comprehensive analysis). For polyethylene, we calculate difference in energies of all-trans and hairpin conformers of short oligomers with the reference CCSD(T) energies taken from ref 58. For polythiophene tetramer, we compare energies of several conformations sampling inter-ring dihedrals relative to the planar one. Finally, for P3HT monomer, we consider a set of low-energy conformers. According to Table 2, CAM-B3LYP-D3 is the most accurate density functional for the considered datasets, having deviations from the reference calculations well below the "chemical accuracy" level of 1 kcal/mol ≈ 43 meV. The basis set 6-311G* seems to provide a good trade-off between accuracy and numerical efficiency, having only several millielectronvolts difference from 6-311+G(3df,2p), which is substantially smaller than variations of conformer energies upon change of density functional. For

DOI: 10.1021/acs.jpcc.7b11271
J. Phys. Chem. C 2018, 122, 9141−9151

Table 2. Assessment of Density Functionals for P3HT Fragments: Polyethylene (PE), Polythiophene (PT), and P3HT Monomer (M)[a]

	PE	PT	M
dataset size	6	7	72
Fixed Basis Set 6-311G*			
CAM-B3LYP-D3	5	9	5
B3LYP-D3	16	5	12
PBE-MBD	22	23	13
vdW-DF2	19	20	17
LC-ωPBE-D3	50	15	24
ωB97XD	90	16	26
OPLS	118	54	56
CAM-B3LYP	195	9	64
Fixed Functional CAM-B3LYP-D3			
6-311G*	5	9	5
6-311G**	8	8	6
6-311+G(3df,2p)	10	1	12
6-31G*	19	6	6

[a]The entries are the root mean square deviation for conformational energies (relative to the lowest-energy conformer) with respect to the reference CCSD(T)/cc-pVTZ values. All energies are in milli electronvolts. The geometry is fixed at MP2/cc-pVTZ for polyethylene and at CAM-B3LYP-D3/6-311G* for other systems. The details are given in the main text, Table S4, Figure S10, Table S6.

plane-wave basis, both PBE-MBD and vdW-DF2 methods show accuracy comparable with the best hybrid functionals. The former gives slightly better energies and geometries for P3HT monomer (see Table S7), whereas the latter is computationally more efficient for bulk solids. In addition, we have performed geometry comparison for relevant crystals with fully resolved atomic positions: polyethylene,[59] quarterthiophene,[60] and type-2 P3HT,[20] showing the same trend, see Table S8. Consequently, CAM-B3LYP-D3/6-311G*, PBE-MBD, and vdW-DF2 are the three methods used for all subsequent DFT calculations performed in this work. When the results are essentially the same for all three functionals, we use the word "DFT" without specifying a specific functional.

Classical force field simulations are used to obtain the initial guess for geometry of possible P3HT polymorphs as well as to investigate dynamic and kinetic stability of the obtained structures. We use LAMMPS program[61] and optimized potentials for liquid simulations (OPLS)-style[62,63] force field. The parameters are taken from ref 30 with two modifications: we neglect the fifth order coefficient for the inter-ring dihedral and use long-range electrostatics to avoid artifacts in geometry optimization. Comparison with experimental geometries of crystals of oligomers[30] and DFT-optimized geometries obtained in the present work shows that this OPLS force field gives accurate geometries. However, the total energies are inaccurate with the standard deviation exceeding 40 meV/monomer (1 kcal/mol, see Figure S27). MD simulations are performed in NPT ensemble at zero pressure with the artificial periodic dimensions (two for polymer, one for π-stack) uncoupled from barostat. The time step is 1 fs. Geometry relaxation is performed by alternation of conjugated gradients and damped dynamics ("fire" style[64]) to overcome shallow traps on PES.

METHODOLOGY FOR STRUCTURAL SEARCH AND ANALYSIS

To describe the structure of bulk P3HT quantitatively, we coarse-grain it by replacing each monomer by a reduced set of parameters fully characterizing the monomer geometry up to nonessential fluctuations; see Figure 2. This set includes: three

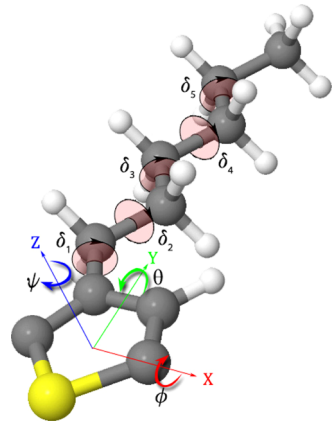

Figure 2. Coarse-grained coordinates of a single P3HT unit: three translations (x, y, z), three rotations (ϕ, θ, ψ), and five dihedrals ($\delta_1 \equiv \delta$, δ_2, ..., δ_5).

Cartesian coordinates (x, y, z) of the center of the thiophene ring, three Euler's angles (ϕ, θ, ψ) rotating the thiophene ring from a canonical orientation to the actual one, and five dihedrals (δ_1, ..., δ_5) defining conformation of the side chain. This parameterization reduces the coordinate space from 25 × 3 correlated Cartesian coordinates per monomer to 11 nearly independent parameters. Only three of them show nontrivial dynamics at room temperature: x, ϕ, and $\delta \equiv \delta_1$. The other eight coordinates include four low-amplitude motions along y, z, θ, and ψ and four quasi-discrete variables $\delta_{2...5}$. Instead of listing values of these coordinates, it is more convenient to encode all possible combinations of them up to nonessential fluctuations. In particular, all side-chain conformations are fully described by five lowercase letters. Each letter encodes a value of a side-chain dihedral: a (180°), b (−60°), and c (+60°). The dihedral δ is special: we use a for $\delta > 0$ and b for $\delta < 0$ provided that the dihedral is counted from the bridging carbon. Although there are five dihedrals to encode, we omit trailing a-s to avoid long notations; e.g., *aacaa* is cut to *aac* when encoding a side chain with $\delta_1 > 0$, $\delta_3 \approx 60°$, and $\delta_{2,4,5} \approx 180°$. These notations are exemplified in Figure 3. Rigorous definition of all parameters and complete encoding of a monomer are given in Section S1.

To encode a crystal structure with a monomer being the asymmetric unit, we combine the above defined side-chain code of the monomer (lowercase letters) with a code describing orientation of thiophene rings in the unit cell (uppercase letters). For 2 × 2 cell, 16 different structural arrangements of the 4 thiophene rings can be identified (see Table S2) and labeled by 2 capital letters, as shown in Figure 4. In addition, there are two special fully planar cases denoted as *C* and *B*. In summary, any rr-P3HT crystal with 2 × 2 unit cell can be labeled by a string of up to two uppercase letters denoting lattice structural type and up to five lowercase letters encoding conformation of the side chain of the asymmetric unit, e.g., *CBaac* (see Figure S23 for illustration). Importantly, any two low-energy crystals with the same code have nearly the same

DOI: 10.1021/acs.jpcc.7b11271
J. Phys. Chem. C 2018, 122, 9141−9151

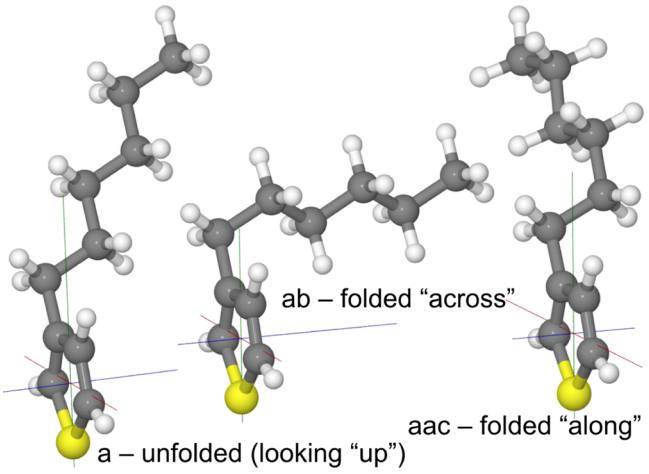

Figure 3. Three conformers dominating in low-energy (*aac*, *ab*) and high-entropy (*a*) structures. Conformer *a* has all dihedrals at their optimal values: $\delta_1 \equiv \delta \sim 110°$ and $\delta_{2...5} \approx 180°$ so that the side chain is directed out of the π-stack plane. Conformer *ab* differs only by $\delta_2 \approx -60°$, resulting in side chain oriented perpendicular to the thiophene ring. Conformer *aac* has $\delta_3 \approx 60°$, and the side chain is directed along the polymer.

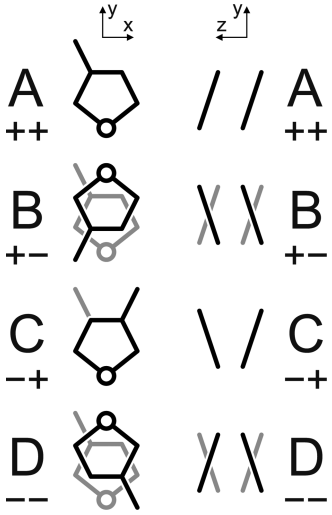

Figure 4. Structural type notations for a 2 × 2 cell. Two signs on the left encode orientation of the foreground polymer relative to the background one in *xy*-plane: forward−backward (sign 1) and up−down (sign 2). Two signs on the right encode orientation of the setting angle for adjacent monomers: coplanar−anticoplanar (sign 3) and eclipsing−staggered (sign 4). For convenience, each pair of signs is encoded by a letter from A to D. Note that only the sign 1 is topological for the molecular dynamics considered in this work (parallel or antiparallel stacking). For illustration, see examples of structural types in Figures S22−S26.

structure, differing mainly by parameters corresponding to large amplitude motions, *x*, φ, and δ.

Predicting the structure of bulk polymers and molecular solids is a challenging problem.[9,54,65] There are two basic approaches: enumerative search[66] and simulation of experimental synthesis and processing.[23,67] The latter approach should give more realistic geometries for each particular experiment, whereas the former one allows for a systematic itemization of all structures possible under a given search constraint. For this reason, we use a combination of both approaches, applying them alternately. We limit our search space to experimentally observed structural motifs, which can be reduced to a four-monomer unit cell (2 × 2). In fact, it is the smallest reasonable cell for P3HT. Indeed, the polythiophene backbone prefers the trans-conformation, setting the minimum period along the polymer chain to two monomers. Commonly assumed polymer reversal symmetry requires that adjacent chains in the π-stack go in the opposite directions (antiparallel stacking), setting the minimum period along the π-stack to two chains. The initial iteration of the search algorithm includes only high-symmetry configurations. Further, we expand the search space by running MD starting from already identified crystalline polymorphs. By high-symmetry we mean a cell with the minimum asymmetric unit, which is a single monomer. Under such constraints, all possible layer symmetry groups are listed in Table S2. The precise algorithm for structural search is detailed in Section S2.

RESULTS AND DISCUSSION

Conformational Preferences of P3HT Fragments. We start our analysis with discussion of conformational preferences of small P3HT fragments to understand basic interatomic interactions determining structure of bulk P3HT. All possible conformers of the side chain can be readily enumerated using hydrogen passivated P3HT monomer. In a polyethylene, each C−C−C−C dihedral alone prefers trans-conformation. The two gauche conformers are low enough in energy, 20 meV, to be important for room-temperature structure of P3HT. In addition, the rotational barrier is only 125 meV, imposing no kinetic constraints for thermal equilibration of the entire PES of side-chain dihedrals.[68] Steric constraints may limit fluctuations of the dihedrals located close to the polymer backbone, such as δ_2, whereas the terminal dihedrals, such as δ_5, are flexible in type-1 interstack packing. The PES for δ_1 is more shallow (Figure S12), with the global minimum at 107°. Yet the cost of planarization is about 65 meV, which is high enough to keep nonplanar conformation also in bulk P3HT, although with substantial spread in values of δ_1 from ∼90 to 180° (Table S11). By taking into account nonbonded interactions, we find their energy sufficient enough to substantially influence conformational preferences. Indeed, in bulk polyethylene the interchain interaction energy is 25−50 meV per carbon (Table S5). As a result, several conformers have their energy smaller or similar to that of the fully unfolded *a*-conformer,[69] which is prevalent in room-temperature crystals. The lowest-energy conformation is *ab* ($\delta_2 \approx -63°$), smaller by 18 meV relative to *a*-conformer. Noticeably, both experimentally derived models of P3HT[11,12] suggest an almost linear side chain, with the only twist at $\delta_2 \approx -133°$. Such value corresponds to a saddle point on PES, and full relaxation of these models as isolated π-stacks by OPLS force field yields *a*-conformer for ref 12 and *ab* conformer for ref 11. Overall, a variety of low-energy conformers for a single monomer should result in combinatorially rich conformational space of bulk P3HT, whereas shallow barriers make these conformers dynamically accessible on a nanosecond scale.

The other nonvibrational intramolecular degree of freedom is the inter-ring dihedral. The geometry of the bithiophene is nonplanar by ∼30° in both trans and cis conformations, in agreement with the experiment[70] (see PES in Figure S8). However, the planarization energy is only 10 meV and is decreasing with the oligomer size, so that thermal fluctuations and nonbonding interactions in bulk P3HT result in a broad distribution of the inter-ring dihedral. Overall, the geometry of

DOI: 10.1021/acs.jpcc.7b11271
J. Phys. Chem. C 2018, 122, 9141−9151

the isolated P3HT polymer is far from being highly symmetric and there is a multitude of close in energy conformations, which should influence intermolecular packing.

Bulk Crystals. To discuss bulk systems, it is important to understand partitioning of their binding energy. Organic molecular crystals show clear separation of various interatomic interactions by strength, concomitant to different levels of structuring.[71] This includes strong covalent bonds forming a molecular framework, weaker intermolecular forces forming a π-stacking order, even weaker undirectional forces connecting π-stacks in a bulk material, and variable-strength noncovalent intramolecular interactions shaping individual molecules.[72] The same picture is expected for P3HT. Indeed, the π-stacking energy is 0.4 eV/monomer for parallel stacking (structure *B*) and 0.5 eV for the antiparallel one (structure *C*). This means that the π-stack is a strongly bound system, although slips along the polymer direction are possible at elevated temperatures.[6] The interstack interaction energy in the reported crystalline geometry[12] optimized by DFT is about 0.1 eV/monomer. In type-1 packing, this energy is distributed among multiple side-chain ends coming in and out of contact upon thermal fluctuations, in contrast to π-stacking energy concentrated in between each pair of polymers constantly. Therefore, the role of interstack interaction in formation of a structural order within π-stacks is small. Indeed, the relaxed geometries of the reported crystal[12] and its isolated π-stack counterpart differ insignificantly; see Table S11. Also, even at 100 K, MD snapshots of isolated π-stacks and crystals show essentially the same intrastack topology (compare Figures S17 and S16). Consequently, a type-1 P3HT crystal can be considered as a system of weakly interacting π-stacks.

Comparison of experimental and calculated geometries for bulk crystals is given in Table 1 (unit cell parameters) and Table S9 (coarse-grained coordinates). Type-2 crystal has no intrinsic disorder because DFT-optimized structure agrees well with the experimental one. There is some discrepancy in x and δ_2 parameters, but upon structural relaxation, the experimental best-fit model[20] readily converges to the DFT-predicted geometry. Type-1 crystals are different, at least for experiments with published atomic positions.[11,12] Both DFT and OPLS force field relaxations of the geometry from ref 12 end up with the optimized structure very similar to the original one, see Table 1. The geometry from ref 11 contains crowded atoms, preventing DFT relaxation, but its formal optimization by OPLS results in the same structure as the one obtained from ref 12. Importantly, experimentally observed cell parameters are much closer to room temperature MD values than to the relaxed geometries, implying that the reported experimental geometries correspond to some average coordinates rather than to a local minimum. Also, the total energy of the DFT-optimized published type-1 crystal is significantly higher than the energy of several polymorphs of isolated π-stack; see e.g., Table S11. Therefore, in the observed type-1 crystals, a substantial intrinsic disorder is present and thus it is natural to expect a pronounced polymorphism for type-1 P3HT.

Polymorphism of π-Stacks at Zero Temperature. On the basis of the search methodology and energy distribution of generated structures (Figure S19), we expect a comprehensive coverage (by force field) of high-symmetry π-stacks within the energy of 150 meV/monomer, as counted from the lowest-energy polymorph. Because the standard deviation of the OPLS energy relative to DFT values is about 50 meV (Figure S27), we expect accurate identification of the lowest-energy polymorphs by DFT within 50 meV range and representative coverage of unfolded conformers up to 200 meV (Table S11). The detailed list of polymorphs is given in the Supporting Information: Table S10 for the OPLS force field, Table S11 for PBE-MBD, and Table S12 for vdW-DF2. A short summary is presented in Table 3 with selected structures illustrated in Figure 5.

Table 3. List of the Lowest-Energy π-Stacks Categorized by Parallel/Antiparallel Stacking and Side-Chain Conformation: Unfolded *a*, Packed Along Polymer *aac*, and Along π-Stacking *ab*[a]

	a		*ab*		*aac*	
Antiparallel	*C*	95	*CA*	17	*CA*	0
	CA′	145	*CB*	54	*CB*	13
Parallel	*BD*	45	*BA*	15	*BA*	44
	BB	79	*BD*	55	*BB*	48

[a]PBE-MBD energies are given in milli electronvolts per monomer relative to the minimum energy of a π-stack (polymorph *CAaac*). *CA′* is the optimized π-stack from ref 12. See the complete list in Table S11.

Analysis of low-energy polymorphs (Table S11) shows two dominating side-chain conformations: *aac* and *ab*; see Figure 3 and Table 3. Both have a tightly packed structure: *aac* with side chains parallel to the polymer and *ab* with side chains perpendicular to the polymer (*abab* at 45 meV is a variation of the latter). Entropically stable unfolded conformers (*a* and *b*) start to appear at much higher energies of 80 meV, except for *BDa* structure at 45 meV, whose exceptional stability will be discussed later. In particular, one of the lowest-energy unfolded polymorphs of antiparallel stacking is the structure with the maximum possible symmetry, structure *C* at 95 meV. This geometry allows for tight packing of unfolded side chains, similar to what is achieved in *BDa* polymorph for parallel polymers. In the experimentally reported crystal,[12] packing of side chains is different so that each of them interacts with four side chains from the adjacent π-stack (C−C distances are 4.0 ± 0.1 Å). Overall, the three conformations *a*, *ab*, and *aac* dominate low-energy polymorphs up to 150 meV (Figure S20). Distribution of lattice types is more uniform, suggesting a relative flexibility of inter-ring dihedrals and π-stacking of thiophene rings, in agreement with the recently proposed model.[6] Steric constraints suppress the *xy*-arrangements A/D and *zy*-arrangements C/D in Figure 4 so that $(B/C)(A/B)$ combinations prevail (Table 3).

Lifting symmetry restrictions of Table S2 neither leads to principally new structures nor changes the overall energy landscape, except for amorphous structures discussed later. Typical symmetry breaking results in modulation of monomer parameters either along the polymer chain or along the π-stacking. Such modulations often lower the energy for the OPLS force field, whereas DFT calculations show that a more symmetric structure is usually more stable, consistent with 2 × 2 unit cell symmetry with the smallest asymmetric unit. Another symmetry readily broken in isolated π-stacks is the symmetry of their two facets ($y > 0$ and $y < 0$) because the side chains attached to the opposite facets do not interact directly with each other. Comprehensive investigation of possible low-symmetry polymorphs is limited by accuracy of the force field.

The translation period of the polymer is 7.80(2) Å for all DFT-optimized polymorphs, implying that the experimentally

DOI: 10.1021/acs.jpcc.7b11271
J. Phys. Chem. C 2018, 122, 9141−9151

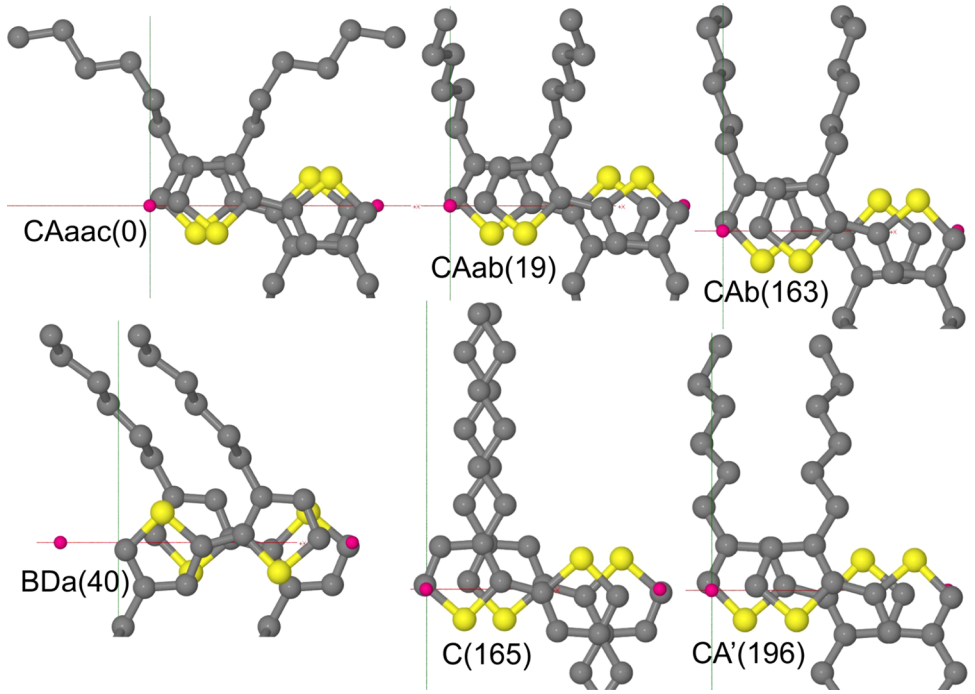

Figure 5. Unit cells of selected polymorphs viewed along *z*-axis. The vdW-DF2 energies in milli electronvolts are given in parentheses. Unit cells are denoted by translation vectors starting at the origin and ending at magenta balls. The *x*- and *y*-axes are marked by red and green colors, respectively.

observed shrinkage to 7.6 Å is caused by thermal disorder. Most of the calculated values of the π-stack period vary from 7.4 to 7.9 Å in consistency with experiments. Extra large values (>8 Å) correspond to large settings angles (>30°), and might contribute to a quenched disorder in bulk P3HT. The dihedral δ for most of polymorphs deviates from the optimal single-molecule value by no more than 20°, corresponding to rather small penalty of about 10 meV. Exceptions from this rule are rare and include the two highest-symmetry structures *C* and *B*, and experimentally derived geometry, even though a bias toward optimal values of dihedrals has been set by the search algorithm. In any case, substantial deviation between experimental and computed geometries of type-1 crystal as well as existence of a number of polymorphs energetically and structurally similar to the experimental one, support the idea that the observed structure is an averaged one, and a multitude of geometrically distinct isoenergetic microstructures may coexist both dynamically due to thermal fluctuations and as a quenched disorder.

Elevated Temperatures. Our present study of P3HT at nonzero temperatures is limited by accuracy of the available force field so that the results should be considered only qualitatively: we are not predicting room-temperature structure but rather investigate how given low-energy polymorphs are transforming at elevated temperatures, to derive generic conclusions applicable for DFT structures as well. Again, type-1 and type-2 crystals behave differently. Type-2 crystal is the lowest-energy polymorph among all known bulk P3HT forms, being more stable than the lowest-energy π-stack by 128 meV/monomer. It is thermally stable at room temperatures under periodic boundary conditions (Figure S18), consistent with the experimentally measured melting temperature of 400 K for long oligomers.[21] In contrast, type-1 crystals and isolated π-stacks undergo order−disorder transition at some temperature below 300 K; see Table S10. For π-stacks, after 1 ns MD at 400 K followed by 1 ns quench, all studied crystalline polymorphs transform into one of four structures identified as a-*CBa*, a-*Ca*, *BDa*, and a-*Ba*, as shown in Figure S16. Here, "a" means amorphous and a-*Ca* means that polymer chains are ordered in the *xy*-plane and disordered in the *yz*-plane (see Figure 4). The dihedral δ_1 is also ordered, whereas the rest of degrees of freedom are disordered within the used 2 × 2 unit cell identification algorithm. This means that at elevated temperatures, side chains melt (except for δ_1), setting angles fluctuate, and polymer chains can slip along *x*-direction. As a result, at room temperature, type-1 semicrystalline rr-P3HT is substantially disordered. An exception is *BDa* polymorph which might preserve its crystalline order at elevated temperatures (the available force field shows no melting even at room temperature). Interestingly, we observe two polymorphs per topological class (parallel/antiparallel stacking). They differ by their setting angle pattern: ordered for a-*CBa*/*BDa* and disordered for a-*Ca*/*Ba* (see Table S10). This result is consistent with the hypothesis of ref 8 that the two optically distinct P3HT phases have similar electronic structure and vibronic couplings but shifted exciton levels due to disorder effects.

Although probing dynamics with DFT is not computationally efficient for the considered systems, some information about PES can be obtained from the vibrational analysis. Here, we calculate vibrational frequencies at Γ-point using density functional perturbation theory. Most of the low-energy polymorphs are stable with respect to infinitesimal deformations at the fixed unit cell (Table S14). Among those with imaginary or prominently low frequencies is the relaxed experimental unit cell in both three- and two-dimensional forms. Recently, vibrational density of states (DOS) was used to distinguish polymorphs of P3HT.[5] In agreement with that work, we observe substantial difference in DOS of structures distinct by a single dihedral, such as *CAab* vs *CAabab* or *CAaac* vs *CAab* (Figure S28). On the other hand, structures with the same side-chain conformation, such as *CAab* vs *BAab* or *CAaac*

DOI: 10.1021/acs.jpcc.7b11271
J. Phys. Chem. C 2018, 122, 9141−9151

vs *CBaac*, have very similar DOS except for that in the low-frequency region. The difference between three- and two-dimensional forms is even smaller (crystal vs π-stack in Figure S28). The calculated elasticity tensor (Table S15) is positive definite for low-energy structures, although the smallest eigenvalue is typically less than 1 GPa (it corresponds to *XZ*-deformation).

CONCLUSIONS

Establishing relationships between structure and electronic properties for organic semiconductors is pivotal for a number of optoelectronic technologies based on these materials. This task is complicated owing to materials' softness and multiple competing interactions ensuring a range of feasible and frequently coexisting chain packings spanning from highly ordered microcrystals to completely amorphous structures. Such diversity is of critical importance for optical and charge carrier transport properties. Even for the most studied P3HT polymer, available experimental and theoretical reports do not accurately resolve individual atom positions across packed microstructures in the bulk material. In the modeling arena, addressing this question requires a combination of a variety of electronic structure and classical MD approaches encompassing different scales. In addition, to account for enormous conformational variety of chain packings, structural modeling should be supplemented with an exhaustive and systematic search protocol for low-energy crystalline polymorphs. All of these components underscore our present modeling study.

Methodologically, we have performed extensive benchmarking of density functionals to CCSD(T) results for small P3HT fragments. In particular, we show that CAM-B3LYP-D3/6-311G* is among the most accurate computationally inexpensive DFT methods for P3HT, whereas PBE-MBD and vdW-DF2 functionals are accurate enough to be used for calculations with periodic boundary conditions. The generated symmetry-enumerated set of polymorphs can be further used as a seeding set for a more thorough search and for benchmarking of density functionals and force fields.

From our analysis, it follows that rr-P3HT is a statistically frustrated material in a sense that there are competing interatomic interactions of comparable strength but with inconsistent optimal geometries, which is typical for glass formers.[73] This leads to a broad variety of nearly isoenergetic geometries with distinct ordering. In particular, side-chain dihedrals alone prefer the trans-conformation but noncovalent interactions in P3HT environment minimize energy in folded conformations. The inter-ring dihedral prefers nonplanar conformation, but the π-stacking stabilizes the planar one. As a result of such frustration, we have about 10 lowest-energy high-symmetry two-dimensional π-stack polymorphs within the energy window of only 2 meV per atom, i.e., about 50 meV/monomer. All of these crystals have topologically different geometries and are kinetically stable at 200 K. In three dimensions, we naturally expect a combinatorially large number of nearly isoenergetic bulk structures, which can be obtained by piling up π-stacks on top of each other in the type-1 packing. Here, we do not observe any specific interstack interaction influencing intrastack structure so that the obtained ensemble of π-stacks should be representative of type-1 bulk P3HT.

All of the observed structures can be accurately parameterized by the proposed coarse-grained model involving 11 nearly independent degrees of freedom per monomer, including 3 translations, 3 rotations, and 5 dihedrals. The lowest-energy polymorphs adopt a 2 × 2 unit cell with the smallest possible asymmetric unit. This symmetry can be broken at elevated energies and temperatures by slight modulation of monomer geometry. At room temperature, side chains melt into a glass former, although π-stacking order persists. Subsequently, we observe upon cooling a partially ordered structure corresponding to the so called "limit disordered" polymer model.[9] This disorder should be taken into account in best-fit modeling of experimental structural data because existing "limit ordered" models do not correspond to a low-energy or thermally stable structure. A modeling of the room-temperature P3HT structure is currently limited by insufficient accuracy of available force fields. Using the published force field, at elevated temperatures, we have obtained four distinct semicrystalline π-stacks: two for parallel and two for antiparallel π-stacking. One of these two phases is a more ordered form of the other one, in agreement with the hypothesis suggested in ref 8.

We observe no preference between parallel and antiparallel stacking of P3HT chains. This should lead to a static disorder in self-assembled π-stacks, similar to that introduced by regio-randomness of P3HT chains. Consequently, it is interesting to see in practice if π-stack-regular P3HT would show an improved crystalline order. Another morphology with reduced disorder is a fully interdigitated one: it is substantially lower in energy than a type-1 structure, which however is stable at any temperature studied here.

In summary, this work provides a systematic modeling study of low-energy high-symmetry structures of bulk P3HT polymer. The obtained polymorphs can be used as a seeding set for a more comprehensive exploration of the configuration space, as a training set for optimization of density functionals and force fields, as well as for interpretation of experimental data with incompletely resolved molecular structure. Some of the two-dimensional structures can be energetically favorable in nonbulk forms,[74] in particular at oriented planar interfaces with well-ordered materials.[75−77]

ASSOCIATED CONTENT

Supporting Information

The Supporting Information is available free of charge on the ACS Publications website at DOI: 10.1021/acs.jpcc.7b11271.

Atomic coordinates for DFT-optimized polymorphs (ZIP)

Details of structural analysis (Figure S1, Tables S1 and S2); structure prediction algorithm (Figures S2−S4); polyethylene oligomers (Tables S3 and S4, Figures S5−S7); elastic constants and vibrational frequencies (Tables S14 and S15, Figures S28 and S29) (PDF)

AUTHOR INFORMATION

Corresponding Authors

*E-mail: a.zhugayevych@skoltech.ru. Phone: +7 495 2801481 (A.Z.).

*E-mail: serg@lanl.gov (S.T.).

ORCID

Andriy Zhugayevych: 0000-0003-4713-1289

Sergei Tretiak: 0000-0001-5547-3647

Notes

The authors declare no competing financial interest.

DOI: 10.1021/acs.jpcc.7b11271
J. Phys. Chem. C 2018, 122, 9141−9151

■ ACKNOWLEDGMENTS

This work is funded by Volkswagen Foundation (A115678). A.Z. acknowledges also financial support by Russian Science Foundation (16-13-00111). This work was performed, in part, at the Center for Integrated Nanotechnologies, an Office of Science User Facility operated for the U.S. Department of Energy (DOE) Office of Science by Los Alamos National Laboratory (Contract DE-AC52-06NA25396) and Sandia National Laboratories (Contract DE-AC04-94AL85000).

■ REFERENCES

(1) Brinkmann, M.; Hartmann, L.; Kayunkid, N.; Djurado, D. In *P3HT Revisited - From Molecular Scale to Solar Cell Devices*; Ludwigs, S., Ed.; Springer: Berlin, 2014; pp 83−106.
(2) Tremel, K.; Ludwigs, S. In *P3HT Revisited - From Molecular Scale to Solar Cell Devices*; Ludwigs, S., Ed.; Springer: Berlin, 2014; pp 39−82.
(3) Wirix, M. J. M.; Bomans, P. H. H.; Friedrich, H.; Sommerdijk, N. A. J. M.; de With, G. Three-Dimensional Structure of P3HT Assemblies in Organic Solvents Revealed by Cryo-TEM. *Nano Lett.* **2014**, *14*, 2033−2038.
(4) Agbolaghi, S.; Zenoozi, S. A Comprehensive Review on Poly(3-alkylthiophene)-based Crystalline Structures, Protocols and Electronic Applications. *Org. Electron.* **2017**, *51*, 362−403.
(5) Harrelson, T. F.; Cheng, Y. Q.; Li, J.; Jacobs, I. E.; Ramirez-Cuesta, A. J.; Faller, R.; Moule, A. J. Identifying Atomic Scale Structure in Undoped/Doped Semicrystalline P3HT Using Inelastic Neutron Scattering. *Macromolecules* **2017**, *50*, 2424−2435.
(6) Bohle, A.; Dudenko, D.; Koenen, N.; Sebastiani, D.; Allard, S.; Scherf, U.; Spiess, H. W.; Hansen, M. R. A Generalized Packing Model for Bulk Crystalline Regioregular Poly(3-alkylthiophenes) with Extended Side Chains. *Macromol. Chem. Phys.* **2017**, No. 1700266.
(7) Kilina, S.; Batista, E. R.; Yang, P.; Tretiak, S.; Saxena, A.; Martin, R. L.; Smith, D. L. Electronic Structure of Self-Assembled Amorphous Polyfluorenes. *ACS Nano* **2008**, *2*, 1381−1388.
(8) Panzer, F.; Sommer, M.; Bässler, H.; Thelakkat, M.; Köhler, A. Spectroscopic Signature of Two Distinct H-Aggregate Species in Poly(3-hexylthiophene). *Macromolecules* **2015**, *48*, 1543−1553.
(9) De Rosa, C.; Auriemma, F. *Handbook of Polymer Crystallization*; Wiley, 2013; pp 31−72.
(10) Xiao, X.; Wang, Z.; Hu, Z.; He, T. Single Crystals of Polythiophene with Different Molecular Conformations Obtained by Tetrahydrofuran Vapor Annealing and Controlling Solvent Evaporation. *J. Phys. Chem. B* **2010**, *114*, 7452−7460.
(11) Kayunkid, N.; Uttiya, S.; Brinkmann, M. Structural Model of Regioregular Poly(3-hexylthiophene) Obtained by Electron Diffraction Analysis. *Macromolecules* **2010**, *43*, 4961−4967.
(12) Dudenko, D.; Kiersnowski, A.; Shu, J.; Pisula, W.; Sebastiani, D.; Spiess, H. W.; Hansen, M. R. A Strategy for Revealing the Packing in Semicrystalline π-Conjugated Polymers: Crystal Structure of Bulk Poly-3-hexyl-thiophene (P3HT). *Angew. Chem., Int. Ed.* **2012**, *51*, 11068−11072.
(13) Rivnay, J.; Mannsfeld, S. C. B.; Miller, C. E.; Salleo, A.; Toney, M. F. Quantitative Determination of Organic Semiconductor Microstructure from the Molecular to Device Scale. *Chem. Rev.* **2012**, *112*, 5488−5519.
(14) Lan, Y.-B.; Sher, P.-H.; Lee, C.-K.; Pao, C.-W.; Tsao, C.-S.; Huang, Y.-C.; Huang, P.-T.; Wu, C.-I.; Wang, J.-K. Revealing Ordered Polymer Packing during Freeze-Drying Fabrication of a Bulk Heterojunction Poly(3-hexylthiophene-2,5-diyl):[6,6]-Phenyl-C61-butyric Acid Methyl Ester Layer: In Situ Optical Spectroscopy, Molecular Dynamics Simulation, and X-ray Diffraction. *J. Phys. Chem. C* **2017**, *121*, 14826−14834.
(15) Nieuwendaal, R. C.; Snyder, C. R.; DeLongchamp, D. M. Measuring Order in Regioregular Poly(3-hexylthiophene) with Solid-State 13C CPMAS NMR. *ACS Macro Lett.* **2014**, *3*, 130−135.
(16) Thurn-Albrecht, T.; Thomann, R.; Heinzel, T.; Hugger, S. Semicrystalline Morphology in Thin Films of Poly(3-Hexylthiophene). *Colloid Polym. Sci.* **2004**, *282*, 932−938.
(17) Joshi, S.; Pingel, P.; Grigorian, S.; Panzner, T.; Pietsch, U.; Neher, D.; Forster, M.; Scherf, U. Bimodal Temperature Behavior of Structure and Mobility in High Molecular Weight P3HT Thin Films. *Macromolecules* **2009**, *42*, 4651−4660.
(18) Wu, Z.; Petzold, A.; Henze, T.; Thurn-Albrecht, T.; Lohwasser, R. H.; Sommer, M.; Thelakkat, M. Temperature and Molecular Weight Dependent Hierarchical Equilibrium Structures in Semiconducting Poly(3-hexylthiophene). *Macromolecules* **2010**, *43*, 4646−4653.
(19) Thankaraj Salammal, S.; Dai, S.; Pietsch, U.; Grigorian, S.; Koenen, N.; Scherf, U.; Kayunkid, N.; Brinkmann, M. Influence of Alkyl Side Chain Length on the In-Plane Stacking of Room Temperature and Low Temperature Cast Poly(3-Alkylthiophene) Thin Films. *Eur. Polym. J.* **2015**, *67*, 199−212.
(20) Rahimi, K.; Botiz, I.; Stingelin, N.; Kayunkid, N.; Sommer, M.; Koch, F. P. V.; Nguyen, H.; Coulembier, O.; Dubois, P.; Brinkmann, M.; et al. Controllable Processes for Generating Large Single Crystals of Poly(3-hexylthiophene). *Angew. Chem., Int. Ed.* **2012**, *51*, 11131−11135.
(21) Koch, F. P. V.; Heeney, M.; Smith, P. Thermal and Structural Characteristics of Oligo(3-hexylthiophene)s (3HT)n, n = 4-36. *J. Am. Chem. Soc.* **2013**, *135*, 13699−13709.
(22) Poelking, C.; Daoulas, K.; Troisi, A.; Andrienko, D. In *P3HT Revisited - From Molecular Scale to Solar Cell Devices*; Ludwigs, S., Ed.; Springer: Berlin, 2014; pp 139−180.
(23) Alexiadis, O.; Mavrantzas, V. G. All-Atom Molecular Dynamics Simulation of Temperature Effects on the Structural, Thermodynamic, and Packing Properties of the Pure Amorphous and Pure Crystalline Phases of Regioregular P3HT. *Macromolecules* **2013**, *46*, 2450−2467.
(24) Tummala, N. R.; Risko, C.; Bruner, C.; Dauskardt, R. H.; Brédas, J.-L. Entanglements in P3HT and Their Influence on Thin-Film Mechanical Properties: Insights from Molecular Dynamics Simulations. *J. Polym. Sci., Part B: Polym. Phys.* **2015**, *53*, 934−942.
(25) Miura, T.; Ito, T.; Shimomura, T. Molecular Dynamics Simulation on the Nanofiber Formation of Conducting Polymers in Solutions. *Mol. Cryst. Liq. Cryst.* **2016**, *629*, 248−253.
(26) Jones, M. L.; Jankowski, E. Computationally Connecting Organic Photovoltaic Performance to Atomistic Arrangements and Bulk Morphology. *Mol. Simul.* **2017**, 756−773.
(27) Xie, W.; Sun, Y. Y.; Zhang, S. B.; Northrup, J. E. Structure and Sources of Disorder in Poly(3-Hexylthiophene) Crystals Investigated by Density Functional Calculations with van der Waals Interactions. *Phys. Rev. B* **2011**, *83*, No. 184117.
(28) Tsumuraya, T.; Song, J.-H.; Freeman, A. J. Linear Optical Properties and Electronic Structures of Poly(3-Hexylthiophene) and Poly(3-Hexylselenophene) Crystals From First Principles. *Phys. Rev. B* **2012**, *86*, No. 075114.
(29) Marcon, V.; Raos, G. Molecular Modeling of Crystalline Oligothiophenes: Testing and Development of Improved Force Fields. *J. Phys. Chem. B* **2004**, *108*, 18053−18064.
(30) Moreno, M.; Casalegno, M.; Raos, G.; Meille, S. V.; Po, R. Molecular Modeling of Crystalline Alkylthiophene Oligomers and Polymers. *J. Phys. Chem. B* **2010**, *114*, 1591−1602.
(31) Poelking, C.; Andrienko, D. Effect of Polymorphism, Regioregularity and Paracrystallinity on Charge Transport in Poly(3-hexylthiophene) [P3HT] Nanofibers. *Macromolecules* **2013**, *46*, 8941−8956.
(32) Bhatta, R. S.; Yimer, Y. Y.; Perry, D. S.; Tsige, M. Improved Force Field for Molecular Modeling of Poly(3-hexylthiophene). *J. Phys. Chem. B* **2013**, *117*, 10035−10045.
(33) Łużny, W.; Piwowarczyk, K. Molecular Dynamics Simulations of Poly(Alkylthiophenes): An Overall View of Some Recent Results. *Synth. Met.* **2013**, *179*, 1−9.
(34) Adler, T. B.; Werner, H.-J. An Explicitly Correlated Local Coupled Cluster Method For Calculations of Large Molecules Close to the Basis Set Limit. *J. Chem. Phys.* **2011**, *135*, No. 144117.

DOI: 10.1021/acs.jpcc.7b11271
J. Phys. Chem. C 2018, 122, 9141−9151

(35) Werner, H.-J.; Knowles, P. J.; Knizia, G.; Manby, F. R.; Schütz, M. Molpro: a General-Purpose Quantum Chemistry Program Package. *Wiley Interdiscip. Rev.: Comput. Mol. Sci.* **2012**, *2*, 242−253.
(36) Werner, H.-J.; Knowles, P. J.; Knizia, G.; Manby, F. R.; Schütz, M.; Celani, P.; Györffy, W.; Kats, D.; Korona, T.; et al. *MOLPRO*, version 2015.1, 2015. http://www.molpro.net.
(37) Dunning, T. H. Gaussian Basis Sets for Use in Correlated Molecular Calculations. I. The Atoms Boron through Neon and Hydrogen. *J. Chem. Phys.* **1989**, *90*, 1007−1023.
(38) Woon, D. E.; Dunning, T. H. J. Gaussian Basis Sets for Use in Correlated Molecular Calculations. III. The Atoms Aluminum through Argon. *J. Chem. Phys.* **1993**, *98*, 1358−1371.
(39) Zhugayevych, A.; Postupna, O.; Wang, H.-L.; Tretiak, S. Modification of Optoelectronic Properties of Conjugated Oligomers due to Donor/Acceptor Functionalization: DFT Study. *Chem. Phys.* **2016**, *481*, 133−143.
(40) Zhugayevych, A.; Tretiak, S. Theoretical Description of Structural and Electronic Properties of Organic Photovoltaic Materials. *Annu. Rev. Phys. Chem.* **2015**, *66*, 305−330.
(41) Zhang, C.-R.; Sears, J. S.; Yang, B.; Aziz, S. G.; Coropceanu, V.; Bredas, J.-L. Theoretical Study of the Local and Charge-Transfer Excitations in Model Complexes of Pentacene-C60 Using Tuned Range-Separated Hybrid Functionals. *J. Chem. Theory Comput.* **2014**, *10*, 2379−2388.
(42) Grimme, S.; Hansen, A.; Brandenburg, J. G.; Bannwarth, C. Dispersion-Corrected Mean-Field Electronic Structure Methods. *Chem. Rev.* **2016**, *116*, 5105−5154.
(43) Grimme, S.; Ehrlich, S.; Goerigk, L. Effect of the Damping Function in Dispersion Corrected Density Functional Theory. *J. Comput. Chem.* **2011**, *32*, 1456−1465.
(44) Chai, J.-D.; Head-Gordon, M. Long-Range Corrected Hybrid Density Functionals with Damped Atom-Atom Dispersion Corrections. *Phys. Chem. Chem. Phys.* **2008**, *10*, 6615−6620.
(45) Sure, R.; Brandenburg, J. G.; Grimme, S. Small Atomic Orbital Basis Set First-Principles Quantum Chem. Methods for Large Molecular and Periodic Systems: A Critical Analysis of Error Sources. *ChemistryOpen* **2016**, *5*, 94−109.
(46) Frisch, M. J.; Trucks, G. W.; Schlegel, H. B.; Scuseria, G. E.; Robb, M. A.; Cheeseman, J. R.; Scalmani, G.; Barone, V.; Mennucci, B.; et al. *Gaussian 09*, revision A.1; Gaussian Inc.: Wallingford, CT, 2009.
(47) Lee, K.; Murray, E. D.; Kong, L.; Lundqvist, B. I.; Langreth, D. C. Higher-Accuracy van der Waals Density Functional. *Phys. Rev. B* **2010**, *82*, No. 081101.
(48) Klimeš, J.; Bowler, D. R.; Michaelides, A. Van der Waals Density Functionals Applied to Solids. *Phys. Rev. B* **2011**, *83*, No. 195131.
(49) Ambrosetti, A.; Reilly, A. M.; DiStasio, R. A. J.; Tkatchenko, A. Long-Range Correlation Energy Calculated from Coupled Atomic Response Functions. *J. Chem. Phys.* **2013**, *140*, No. 18A508.
(50) Perdew, J. P.; Yue, W. Accurate and Simple Density Functional For the Electronic Exchange Energy: Generalized Gradient Approximation. *Phys. Rev. B* **1986**, *33*, 8800−8802.
(51) Murray, E. D.; Lee, K.; Langreth, D. C. Investigation of Exchange Energy Density Functional Accuracy for Interacting Molecules. *J. Chem. Theory Comput.* **2009**, *5*, 2754−2762.
(52) Brown-Altvater, F.; Rangel, T.; Neaton, J. B. Ab Initio Phonon Dispersion in Crystalline Naphthalene Using van der Waals Density Functionals. *Phys. Rev. B* **2016**, *93*, No. 195206.
(53) Pham, T. H.; Ramprasad, R.; Nguyen, H.-V. Density-Functional Description of Polymer Crystals: A Comparative Study of Recent van der Waals Functionals. *J. Chem. Phys.* **2016**, *144*, No. 214905.
(54) Beran, G. J. O. Modeling Polymorphic Molecular Crystals with Electronic Structure Theory. *Chem. Rev.* **2016**, *116*, 5567−5613.
(55) Perdew, J. P.; Burke, K.; Ernzerhof, M. Generalized Gradient Approximation Made Simple. *Phys. Rev. Lett.* **1996**, *77*, 3865−3868.
(56) Kresse, G.; Furthmüller, J. Efficient Iterative Schemes for Ab Initio Total-Energy Calculations Using a Plane-Wave Basis Set. *Phys. Rev. B* **1996**, *54*, 11169−11186.
(57) Kresse, G.; Joubert, D. From Ultrasoft Pseudopotentials to the Projector Augmented-Wave Method. *Phys. Rev. B* **1999**, *59*, 1758−1775.
(58) Byrd, J. N.; Bartlett, R. J.; Montgomery, J. A. At What Chain Length do Unbranched Alkanes Prefer Folded Conformations? *J. Phys. Chem. A* **2014**, *118*, 1706−1712.
(59) Busing, W. R. X-ray Diffraction Study of Disorder in Allied Spectra-1000 Polyethylene Fibers. *Macromolecules* **1990**, *23*, 4608−4610.
(60) Siegrist, T.; Kloc, C.; Laudise, R. A.; Katz, H. E.; Haddon, R. C. Crystal Growth, Structure, and Electronic Band Structure of α-4T Polymorphs. *Adv. Mater.* **1998**, *10*, 379−382.
(61) Plimpton, S. Fast Parallel Algorithms for Short-Range Molecular Dynamics. *J. Comput. Phys.* **1995**, *117*, 1−19.
(62) Jorgensen, W. L.; Maxwell, D. S.; Tirado-Rives, J. Development and Testing of the OPLS All-Atom Force Field on Conformational Energetics and Properties of Organic Liquids. *J. Am. Chem. Soc.* **1996**, *118*, 11225−11236.
(63) Ponder, J. W. TINKER 7.1. http://dasher.wustl.edu/tinker.
(64) Bitzek, E.; Koskinen, P.; Gähler, F.; Moseler, M.; Gumbsch, P. Structural Relaxation Made Simple. *Phys. Rev. Lett.* **2006**, *97*, No. 170201.
(65) Brandenburg, J. G.; Grimme, S. Organic Crystal Polymorphism: a Benchmark for Dispersion-Corrected Mean-Field Electronic Structure Methods. *Acta Crystallogr., Sect. B: Struct. Sci., Cryst. Eng. Mater.* **2016**, *72*, 502−513.
(66) Sharma, V.; Wang, C.; Lorenzini, R. G.; Ma, R.; Zhu, Q.; Sinkovits, D. W.; Pilania, G.; Oganov, A. R.; Kumar, S.; Sotzing, G. A.; et al. Rational Design of All Organic Polymer Dielectrics. *Nat. Commun.* **2014**, *5*, No. 4845.
(67) Jones, M. L.; Huang, D. M.; Chakrabarti, B.; Groves, C. Relating Molecular Morphology to Charge Mobility in Semicrystalline Conjugated Polymers. *J. Phys. Chem. C* **2016**, *120*, 4240−4250.
(68) Siu, S. W. I.; Pluhackova, K.; Böckmann, R. A. Optimization of the OPLS-AA Force Field for Long Hydrocarbons. *J. Chem. Theory Comput.* **2012**, *8*, 1459−1470.
(69) Baggioli, A.; Famulari, A. On the Inter-Ring Torsion Potential of Regioregular P3HT: a First Principles Reexamination with Explicit Side Chains. *Phys. Chem. Chem. Phys.* **2014**, *16*, 3983−3994.
(70) Samdal, S.; Samuelsen, E. J.; Volden, H. V. Molecular Conformation of 2,2′-Bithiophene Determined by Gas Phase Electron Diffraction and Ab Initio Calculations. *Synth. Met.* **1993**, *59*, 259−265.
(71) van der Poll, T. S.; Zhugayevych, A.; Chertkov, E.; Bakus, R. C.; Coughlin, J. E.; Teat, S. J.; Bazan, G. C.; Tretiak, S. Polymorphism of Crystalline Molecular Donors for Solution-Processed Organic Photovoltaics. *J. Phys. Chem. Lett.* **2014**, *5*, 2700−2704.
(72) Coughlin, J. E.; Zhugayevych, A.; Bakus, R. C.; van der Poll, T. S.; Welch, G. C.; Teat, S. J.; Bazan, G. C.; Tretiak, S. A Combined Experimental and Theoretical Study of Conformational Preferences of Molecular Semiconductors. *J. Phys. Chem. C* **2014**, *118*, 15610−15623.
(73) Zhugayevych, A.; Lubchenko, V. Electronic Structure and the Glass Transition in Pnictide and Chalcogenide Semiconductor Alloys. I. The Formation of the pp Sigma-Network. *J. Chem. Phys.* **2010**, *133*, No. 234503.
(74) Diao, Y.; Lenn, K. M.; Lee, W.-Y.; Blood-Forsythe, M. A.; Xu, J.; Mao, Y.; Kim, Y.; Reinspach, J. A.; Park, S.; Aspuru-Guzik, A.; et al. Understanding Polymorphism in Organic Semiconductor Thin Films through Nanoconfinement. *J. Am. Chem. Soc.* **2014**, *136*, 17046−17057.
(75) Jones, A. O. F.; Chattopadhyay, B.; Geerts, Y. H.; Resel, R. Substrate-Induced and Thin-Film Phases: Polymorphism of Organic Materials on Surfaces. *Adv. Funct. Mater.* **2016**, *26*, 2233−2255.
(76) Zhai, L.; Khondaker, S. I.; Thomas, J.; Shen, C.; McInnis, M. Ordered Conjugated Polymer Nano- and Microstructures: Structure Control for Improved Performance of Organic Electronics. *Nano Today* **2014**, *9*, 705−721.
(77) Anokhin, D. V.; Leshanskaya, L. I.; Piryazev, A. A.; Susarova, D. K.; Dremova, N. N.; Shcheglov, E. V.; Ivanov, D. A.; Razumov, V. F.; Troshin, P. A. Towards Understanding the Behavior of Indigo Thin

DOI: 10.1021/acs.jpcc.7b11271
J. Phys. Chem. C 2018, 122, 9141−9151

Films in Organic Field-Effect Transistors: a Template Effect of the Aliphatic Hydrocarbon Dielectric on the Crystal Structure and Electrical Performance of the Semiconductor. *Chem. Commun.* **2014**, *50*, 7639−7641.

DOI: 10.1021/acs.jpcc.7b11271
J. Phys. Chem. C 2018, 122, 9141−9151